CHEMISTRY OF MATERIALS

ARTICLE

pubs.acs.org/cm

Weak Acid−Base Interaction Induced Assembly for the Synthesis of Diverse Hollow Nanospheres

Guang-Hui Wang, Qiang Sun, Rong Zhang, Wen-Cui Li, Xiang-Qian Zhang, and An-Hui Lu*

State Key Laboratory of Fine Chemicals, School of Chemical Engineering, Dalian University of Technology, Dalian 116024, People's Republic of China

Supporting Information

ABSTRACT: We have established a novel and generalizable hydrothermal synthesis for diverse hollow nanospheres, which cover polymer, carbon, graphitic carbon, and metal-doped carbon hollow nanospheres. The synthesis principle is based on the weak acid−base interaction ($-COO^-/NH_4^+/-COO^-$) induced assembly. That is, the ammonium cations from the reactant ammonia act as a trigger for the assembly of COO^- group-containing polymer around surfactant oleic acid micelles through the weak interaction between carboxylate anion and ammonium ion. Consequently, hollow polymer nanospheres (HPSs) with diameters ranging from 100 to 200 nm and hollow core sizes ranging from 30 to 80 nm can be synthesized. It was determined that approximately 61% of the added amount of NH_3 participates is retained in the HPS product. Taking these HPSs as the precursor, hollow carbon nanospheres (HCSs) with tunable surface areas can be obtained by varying the preparation conditions. More importantly, owing to the presence of the COO^- functional groups, a wide range of metal cations (e.g., Fe^{3+} and Ag^+) can be successfully introduced into these HPSs, so that they can then be converted to hollow graphitized nanospheres and Ag-doped catalytically active HCSs.

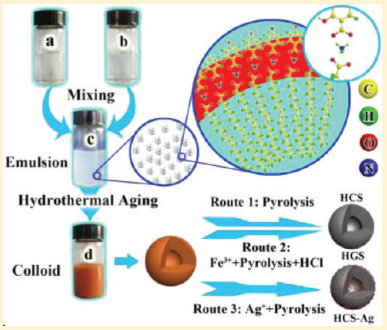

KEYWORDS: carbon, colloidal catalyst, hollow nanospheres, hydrothermal synthesis, weak acid−base interaction

1. INTRODUCTION

The design and fabrication of hollow nanospheres have received considerable attention during the past decade. Particularly, hollow polymer and carbon nanospheres (HPSs, HCSs), which consist of a hollow cavity with tunable size and a functional shell layer, promise wide applications in drug delivery,[1,2] active material encapsulation,[3−6] hydrogen storage,[7] and catalyst supports.[8−10] A variety of chemical syntheses have been reported for the preparation of hollow nanospheres. For example, a straightforward way to prepare HPSs and HCSs is the use of polymer spheres,[11−19] silica,[2−10,20−29] or metals or metal compounds[30−34] as the hard templates. However, it is difficult to obtain HPSs and HCSs with variable functional shell layer and perfect shell structure. Compared to the hard-templating, a relatively simple and feasible pathway is the soft-templating method, which is to encapsulate molecular clusters,[35,36] surfactants,[37−40] block copolymers,[41] or emulsion droplets[42−48] as a core and subsequently induce assembly between the precursor and core to form hollow polymers. Fan and co-workers have synthesized polystyrene hollow nanospheres (less than 50 nm in diameter) through self-assembly between amphiphilic block copolymer (polystyrene-*b*-poly(vinylpyridine)) and 2-[(4′-hydroxybenzyl)azo]benzoic acid.[35] It is problematic to transform the hollow polystyrene nanospheres to HCSs, due to the thermal instability of polystyrene. Li et al. prepared HCSs using glucose as the carbon source and sodium dodecyl sulfate (SDS) as the surfactant under hydrothermal conditions.[37] The obtained HCSs show a wide size distribution ranging from several tens of nanometers to several micrometers. Guo and co-workers reported a method to prepare the poly(*o*-toluidine) hollow spheres using an emulsion as the template without the need for surfactant stabilization.[42] Although the obtained hollow spheres can be converted to HCSs, the products exhibit a broad size distribution from 1 to 8 μm and have an imperfect shell in each sphere.

Nevertheless, the aforementioned syntheses are not effective for the combined control of the size and the functionality of the shell structure of HPSs and HCSs, which may lead to irregular and defective shapes,[37−40,42−46] instability at high temperatures,[35,36,41] or a size beyond micrometers and even cracks in the shell.[36] Hence, one important goal as well as big challenge is to develop a rational and feasible synthesis which can deliver versatile HPSs and HCSs with a functional and crack-free shell structure and tunable sizes on the nanometer scale. In this study, we describe the new synthesis of nanosized HPSs exhibiting controllable sizes and a functionalizable shell through the weak acid−base ($-COO^-/NH_4^+/-COO^-$) interaction induced assembly under hydrothermal conditions. The uniform and functional shells are formed through the polymerization of dihydroxybenzoic acid and formaldehyde in the presence of ammonia. These highly engineered nanospheres can act as a storage reservoir or a nanoreactor, whereas the shell not only provides substantial surface area for reactions, but also facilely

Received: June 26, 2011
Revised: September 2, 2011
Published: September 30, 2011

chelates metal cations through the abundant functional groups in it (being useful for removal of toxic metal ions from soil or water). It is noteworthy that the synthesized HPSs can be further pseudomorphically converted to various carbonaceous nanospheres and highly active colloidal catalysts doped with specific metallic nanoparticles. These materials could offer new opportunities in the field of nanoengineering of targeted colloidal catalysts by taking advantage of their hollow nature.

2. EXPERIMENTAL SECTION

2.1. Chemicals. 2,4-Dihydroxybenzoic acid (DA), hexadecyltrimethylammonium bromide (99%), and Pluronic F127 were obtained from Aldrich. Oleic acid, phenol, formaldehyde, $FeCl_3 \cdot 6H_2O$, $AgNO_3$, 4-nitrophenol, and $NaBH_4$ were obtained from the Sinopharm Chemical Reagent Co. Resorcinol, Na_2CO_3, NaOH, and ammonia solution (25%) were obtained from the Tianjin Kermel Chemical Reagent Co. All chemicals were used as received without any further purification.

2.2. Synthesis of Hollow Polymer Nanospheres. In a typical procedure, 2.5 mmol of 2,4-dihydroxybenzoic acid and 7.5 mmol of formaldehyde were dissolved in 95 mL of deionized water. A 5 mL volume of an aqueous solution containing 56 μL of oleic acid and 180 μL of ammonia solution (25%) was added to the above-prepared solution at 30 °C under slow stirring (100 rpm). The mixture solution was stirred for 30 min to yield a stable emulsion and then transferred into an autoclave hydrothermally aged for 4 h in the temperature range from 100 to 160 °C. The resulting HPSs were retrieved by centrifugation (8000−9000 rpm, 10 min), washed with deionized water and ethanol, and dried at 50 °C for 6 h. Contrast experiments without the use of oleic acid were performed, which resulted in the production of solid polymer spheres (denoted as SPSs).

2.3. Synthesis of Hollow Carbonaceous Nanospheres. HCSs were obtained by heating HPSs to 800 °C with a heating rate of 3 °C min^{-1} and holding them at that temperature for 4 h under a N_2 atmosphere. To increase the surface area of the HCS products, immediately following carbonization at 800 °C for 4 h, the samples were directly heated to 850 °C in CO_2 and held at this temperature for 2 or 3 h, depending on the sample. In the case of obtaining hollow graphitic nanospheres (HGSs), HPSs were first immersed in aqueous $FeCl_3 \cdot 6H_2O$ (0.24 M) overnight to load graphitization catalyst. Subsequently, the polymer was washed with deionized water and ethanol, dried at 50 °C for 6 h, and then pyrolyzed at 850 °C for 3 h under a nitrogen flow. The obtained black powder was treated with concentrated HCl (37%) to remove the leachable Fe-based particles. Finally, the products were obtained after washing and drying.

2.4. Synthesis of Ag-Loaded Hollow Colloidal Catalyst. HPSs were first immersed in aqueous $AgNO_3$ (0.24 M) overnight to load Ag^+ to obtain HPS-Ag. Subsequently, the HPS-Ag was washed with deionized water and ethanol, dried at 50 °C for 6 h, and then pyrolyzed at 400 °C for 2 h under a nitrogen flow to obtain the final HCS-Ag.

2.5. Catalytic Reduction of 4-Nitrophenol. Aqueous solutions of 4-nitrophenol (0.036 mL, 0.01 M) and $NaBH_4$ (0.24 mL, 0.5 M) were added to deionized water (2.25 mL) under constant stirring at room temperature. Subsequently, 0.015 mL of an aqueous dispersion of the catalyst (20 mg of HCS-Ag was homogeneously dispersed in 5 mL of deionized water) was added to the above solution. The mixture was immediately transferred into a quartz cuvette with an optical path length of 1 cm, and UV−vis absorption spectra were recorded to monitor changes in the reaction mixture. The solution was in situ measured every 3 min to obtain successive information about the reaction.

2.6. Characterization. Dynamic light scattering was used for the determination of the average hydrodynamic diameter of the emulsion. The measurements were recorded on a Malvern Instruments Zetasizer Nano-ZS using laser radiation with a wavelength of 633 nm and a power of 4 mW. The scattered light was detected keeping a fixed angle of 90° using a photomultiplier. Transmission electron microscopy (TEM) analyses were carried out with Tecnai $G^2$20S-Twin equipment operating at 200 keV. The samples for TEM analysis were prepared by dipping the carbon-coated copper grids into the ethanol solutions of the products and drying at room temperature. Scanning electron microscopy (SEM) investigations were carried out with a Hitachi S-4800 instrument. Nitrogen adsorption isotherms were measured with a Micromeritics ASAP2020 adsorption analyzer at 77 K. Prior to the measurements, all the samples were degassed at a temperature of 150 °C for 6 h. The specific surface areas were calculated from the adsorption data in the relative pressure range of 0.05−0.3 using the Brunauer−Emmett−Teller (BET) method. The total pore volume was estimated from the amount adsorbed at a relative pressure of 0.90. The micropore volume was calculated using the *t*-plot method. Elemental analysis was carried out using a Perkin-Elmer inductively coupled plasma spectrometer, Optima2000 DV. The mass spectrometric data were acquired on a Q-Tof Micro mass spectrometer (Micromass, Manchester, U.K.) equipped with a Z-spray ionization source. The detected m/z range is from 100 to 1500. The UV−vis spectra were recorded on a UV−vis spectrometer (Techcomp UV 2300) at 25 °C. Thermogravimetric (TG) analysis was conducted on a thermogravimetric analyzer, STA 449 F3 Jupiter (NETZSCH), with a heating rate of 10 °C min^{-1}, and the IR spectrum was collected on a Nicolet 6700 FT-IR spectrometer.

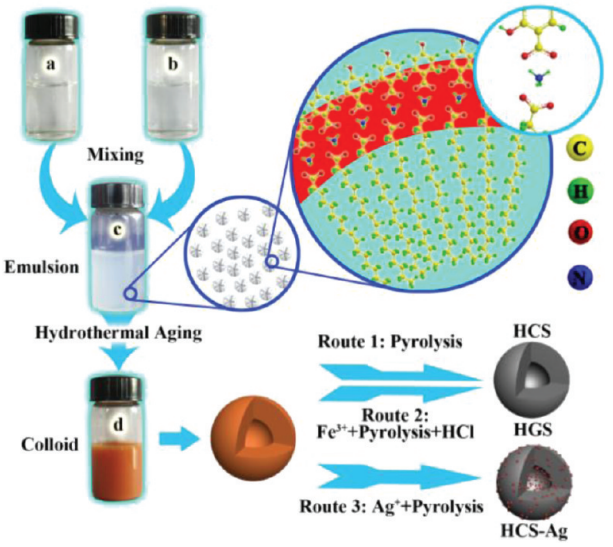

Figure 1. Illustration for the synthesis of diverse hollow polymer, carbon, graphitic, and Ag-doped nanospheres. Photographs of reaction solutions including (a) oleic acid/ammonia (ammonium oleate) solution, (b) DA/formaldehyde solution, (c) the emulsion solution obtained by mixing solutions a and b, and (d) solution c after hydrothermal synthesis.

3. RESULTS AND DISCUSSION

3.1. Synthetic Principle of Hollow Polymer Nanospheres. The synthesis procedure is illustrated in Figure 1. An emulsion solution was prepared by mixing oleic acid/ammonia (forming ammonium oleate) and DA/formaldehyde solution. The dynamic light scattering results are provided in Figure S1 (Supporting Information). Ammonium ions can bridge the organic acids oleic acid and DA by weak acid and base interactions[50] and guide the assembly of DA and formaldehyde around the emulsion of ammonium oleate in the following polymerization process.

Table 1. Synthesis Conditions of Hollow and Solid Polymer Nanospheres

sample	T/t^a (°C/h)	$R^{*\,b}$	$R^{\#\,c}$	$pH_b{}^d$	$pH_a{}^e$
HPS-1	100/4	1.08	0.97	4.02	6.77
HPS-2	120/4	1.08	0.97	4.02	6.77
HPS-3	140/4	1.01	0.90	4.02	6.77
HPS-4	160/4	0.96	0.86	4.02	6.77
HPS-5	120/4			4.29	6.78
SPS	120/4	0.77		4.00	6.85

[a] Hydrothermal reaction temperature and time. [b] Mass ratio between the actual and the theoretical mass of HPSs (the theoretical mass was calculated by assuming that 2.5 mmol of DA reacts with 2.5 mmol of formaldehyde, thus yielding 0.417 g of HPSs). [c] Mass ratio between the actual and the theoretical mass of HPSs (here, the theoretical mass calculated by assuming that 2.5 mmol of DA reacts with 2.5 mmol of formaldehyde and oleic acid surfactants are completely trapped in the polymer product). [d] pH of the reaction solution before hydrothermal synthesis. [e] pH of the reaction solution after hydrothermal synthesis.

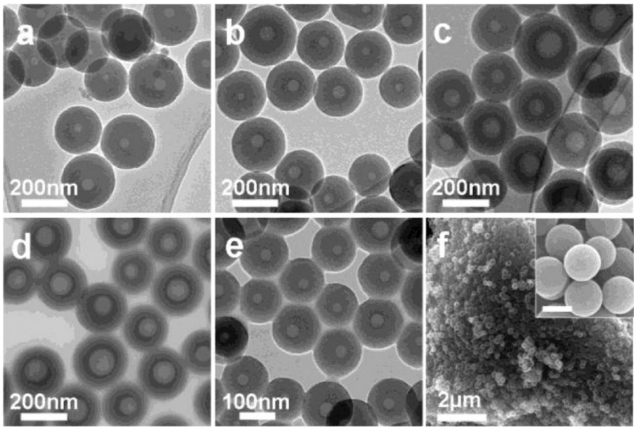

Figure 2. TEM images of (a) HPS-1, (b) HPS-2, (c) HPS-3, (d) HPS-4, and (e) HPS-5. (f) SEM image of HPS-2. The scale bar of the inset is 200 nm.

This principle will be discussed in further detail below. Driven by this interaction, HPSs can be obtained after a hydrothermal synthesis, which can be further engineered to diverse hollow nanostructures such as HCSs, HGSs, and HCS-Ag. This indicates HPSs having a robust and stable core−shell structure.

By varying a hydrothermal temperature from 100 to 160 °C, a series of HPSs, denoted as HPS-*n* (n = 1, 2, 3, 4), were obtained. As seen in Table 1, the pH value of samples HPS-*n* before hydrothermal reactions is ∼4.02. After reaction, the pH value shows a slight increase to ∼6.77. The morphology and size of the products were examined by TEM and SEM. As seen in Figure 2a−d, all products consisted of relatively uniform nanospheres with the approximate size 200 ± 15 nm, as determined from TEM and SEM images by taking at least 100 particles into account. This indicates that the reaction temperature has almost no effect on the sizes of the HPS-*n*. However, the hollow core sizes of the resultant nanospheres increased from 30 ± 5 to 80 ± 5 nm with an increasing reaction temperature from 100 to 160 °C. This phenomenon can be attributed to the volume expansion of the ammonium oleate emulsion at a high temperature. The SEM image (Figure 2f) of HPS-2 shows spheres with a smooth surface and no surface cavities. This proves that these spheres possess perfect interior hollow cores. When using double the amount of oleic acid (112 μL) and 200 μL of ammonia, sample HPS-5 with an average diameter size of 120 ± 15 nm and core diameter of 30 ± 5 nm was obtained (Figure 2e). Thus, an increased amount of oleic acid is beneficial for synthesizing smaller nanospheres containing smaller hollow cores.

To determine whether oleic acid was trapped in the products, we calculated the theoretical mass of HPSs on the basis of the principle that 2.5 mmol of DA reacts with 2.5 mmol of formaldehyde to generate 0.417 g of HPSs. As seen in Table 1, if the mass of oleic acid was not taken into account, the calculated mass ratio R^* was greater than 1, indicating that the monomers were converted to polymer product, especially when the reaction temperature was lower than 140 °C, e.g., samples HPS-1, HPS-2, and HPS-3. By taking the mass of oleic acid into account, the calculated mass ratio $R^{\#}$ of HPS-1 and HPS-2 is close to 1, revealing that oleic acid emulsions are indeed nearly fully encapsulated in the products. The analysis of the upper part of the centrifuged solution of HPS-2 by ESI-MS shows no detectable species in the m/z range from 100 to 1500, indicating all the reactants have been converted to the polymer product. However, higher reaction temperatures (>140 °C) result in smaller R^* and $R^{\#}$ values, indicating the polymer source and surfactant were not fully converted to products at higher reaction temperature.

In addition, supplementary experiments were carried out in the absence of oleic acid while keeping the other reaction conditions the same as those of HPS-2. As a consequence, solid spheres as opposed to hollow ones were obtained. As seen in Figure S2 (Supporting Information), they are mainly composed of large solid polymer spheres with a diameter of 700−1000 nm. This indicates that the oleic acid emulsion is indeed a template to generate the hollow structure. Besides oleic acid, three other surfactants, namely, a nonionic surfactant (Pluronic F127), a cationic surfactant (hexadecyltrimethylammonium bromide), and an anionic surfactant (sodium dodecylbenzenesulfonate), were employed to synthesize HPSs under the same reaction conditions as those of HPS-2. Even by adjusting the amount of ammonia in the range from 100 to 200 μL, they cannot form any stable colloids (Figure S3a-I,II,III, Supporting Information). TEM results show that no hollow nanospheres were found in these noncolloidal products (Figure S3d−f). This suggests that the carboxyl-containing surfactant plays a crucial role in directing the assembly of the hollow nanostructures. When using resorcinol and phenol as the polymer precursor, no HPSs were obtained either (Figure S3a-IV,b,c). These results imply that a precursor containing carboxyl groups is an indispensable factor for achieving hollow nanospheres. It should be emphasized that this is a general route (as shown in Figure 1) toward the synthesis of hollow nanospheres; the synthesis principle described can be extended to other carboxyl-containing surfactants and polymer precursors (see Figure S4, Supporting Information).

An elemental analysis of the as-synthesized HPS-2 (collected after four centrifugations, i.e., washed three times with water and one time with ethanol) revealed that the nitrogen content was ∼4.5 wt %. As the actual collected product of HPS-2 is ∼0.45 g, this sample should thus contain 25 mg of NH_3. During the synthesis, the added NH_3 is ∼41 mg (180 μL, 25%). This indicates that ∼61% of added NH_3 groups as ammonium ions were stably retained in the polymer structures via $-COO^-/NH_4^+/-COO^-$ bonding, since extensive washing did not remove ammonium. The use of other bases such as NaOH and Na_2CO_3 to replace the ammonia solution (keeping other

dx.doi.org/10.1021/cm2018168 |*Chem. Mater.* 2011, 23, 4537–4542

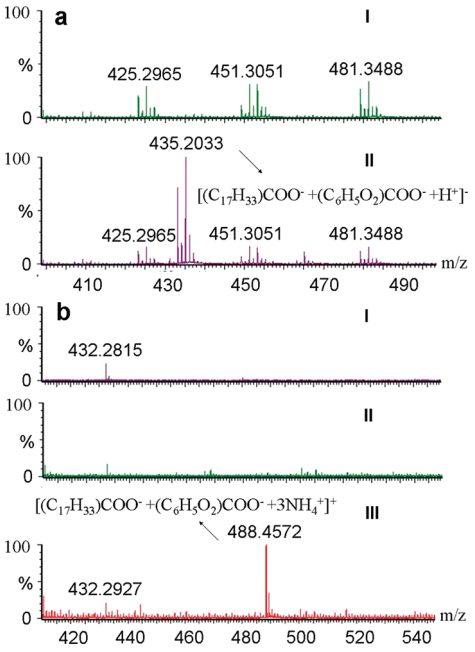

Figure 3. (a) Negative ion ESI mass spectra of (I) oleic acid/NH_3 and (II) oleic acid/NH_3/DA. (b) Positive ion ESI mass spectra of (I) oleic acid/NH_3, (II) DA/NH_3, and (III) oleic acid/NH_3/DA.

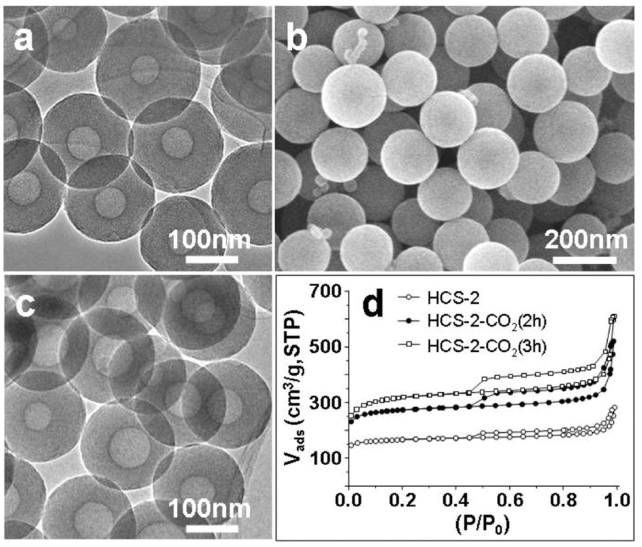

Figure 4. TEM (a) and SEM (b) images of HCS-2. (c) TEM image of HCS-2 after 3 h of CO_2 activation. (d) Nitrogen sorption isotherms of HCS-2, HCS-2-CO_2 (2 h), and HCS-2-CO_2 (3 h).

reaction conditions the same as those of HPS-2) failed to generate HPSs also (Figure S3a-V, Supporting Information). Hence, ammonium ions are indispensable elements for the successful synthesis of hollow nanostructures.

To better understand the nature of the oleic acid/ammonia/DA three-component system, ESI-MS was used for the analysis of oleic acid/ammonia solution and DA solution and their mixture. To eliminate the emulsion of the oleic acid/ammonia/DA system and thus aid an ESI-MS analysis, an extra amount of ammonia was added. As shown in Figure 3a, the spectrum of the three-component mixture contains an intense peak at m/z = 435.2, which corresponds to the species $[(C_{17}H_{33})COO^- + (C_6H_5O_2)COO^- + H^+]^-$. We thus propose that these species were produced from the parent ions $[(C_{17}H_{33})COO^- + (C_6H_5O_2)COO^- + NH_4^+]^-$ at m/z = 452.2 with elimination of neutral NH_3. The collision-induced dissociation (CID) of selected "mixed dimer" ion adducts consisting of two different molecules bound to an NH_4^+ was studied using Q-Tof. The resulting fragment ions indicated that NH_4^+ has a higher affinity for the oleic acid than DA. The positive ion spectra of oleic acid/ammonia/DA solvent (Figure 3b) show a more remarkable peak at m/z = 488.4 (corresponding to $[(C_{17}H_{33})COO^- + (C_6H_5O_2)COO^- + 3NH_4^+]^+$) and also confirm the existence of a weak acid−base interaction. This further proves that ammonium guides the assembly of DA around the emulsion of ammonium oleate via the weak acid−base interaction.

3.2. Versatile Hollow Carbonaceous Nanspheres. The versatility of this synthesis lies in that HPSs can be further converted to HCSs and HGSs at will. For example, hollow carbon HCS-2 can be obtained simply by pyrolysis of its polymer counterpart HPS-2. As shown in Figure 4a,b, the TEM and SEM images of HCS-2 show remarkably uniform spheres and a crack-free hollow core−shell structure. The thermal behavior of HPS-2 was investigated by TG analysis (under nitrogen with a heating rate of 10 °C min^{-1}). For comparison, SPSs as the control sample were analyzed as well. As shown in Figure S5a (Supporting Information), the TG curve of HPS-2 exhibits an obvious weight loss compared to that of SPSs at 300 °C. This can be ascribed to the decomposition of oleic acid embedded inside HPS-2. With the increase in temperature, the two curves are almost parallel to each other, indicating the similar thermal behaviors after the decomposition of oleic acid. The carbon residues for HPS-2 and SPSs are 44% and 51%, respectively.

In addition, the surface area of HCS-2 can be increased by CO_2 activation. TEM (Figure 4c) shows the hollow core−shell nanostructures are still well-retained after CO_2 activation for 3 h. Therefore, the HPSs are structurally stable against carbonization and activation treatment. Physical sorption analyses (Figure 4d) of the samples before and after CO_2 activation suggest that the products have similar pore structures. After CO_2 activation for 2 and 3 h, the surface areas increased from 560 to 920 and 1080 m^2 g^{-1}, respectively, and the total pore volumes increased from 0.30 to 0.49 and 0.58 cm^3 g^{-1}, respectively (Table 2). This reveals that the porosity of the HCSs can be easily tuned by CO_2 activation. Although the shell structures of HPSs and HCSs look similar from Figures 2 and 4, the pore structures of these two samples are different (see the pore size distributions in Figure S6a,b, Supporting Information). The sample HPS-2 has very little porosity and thus a very small surface area (38 m^2 g^{-1}; see Figure S6d).

Due to the presence of abundant carboxylate (see the FT-IR spectrum in Figure S5b, Supporting Information), Fe^{3+} ions can be introduced into HPSs through an ion-exchange process.[49,51] Noticeably, the polymeric shells of the HPSs can be converted to graphitized carbon after pyrolysis in the presence of in situ formed iron nanoparticles, indicating that the HPSs are subject to pseudomorphic transformation during pyrolysis. The SEM and TEM images of HGSs after HCl leaching (Figure 5a−c) show this sample retained a perfect hollow core−shell structure. The high-resolution TEM observation (Figure 5d) reveals that the hollow spheres consist of well-developed nanosized turbostratic graphite structures, and the average thickness of the graphitic sheet is estimated to be 5−10 nm. The diameter and

dx.doi.org/10.1021/cm2018168 |Chem. Mater. 2011, 23, 4537–4542

Table 2. Texture Parameters of HCSs, Activated HCSs, and HGSs[a]

sample	S_{BET} ($m^2\ g^{-1}$)	S_{mic} ($m^2\ g^{-1}$)	V_{mic} ($cm^3\ g^{-1}$)	V_{total} ($cm^3\ g^{-1}$)
HCS-2	560	450	0.21	0.30
HCS-2-CO_2(2 h)	920	740	0.34	0.49
HCS-2-CO_2(3 h)	1080	790	0.36	0.58
HGS-2, HCl	450	270	0.12	0.27

[a] S_{BET} = specific surface area calculated by the BET method, S_{mic} = micropore surface area calculated by the *t*-plot method, V_{mic} = micropore volume calculated by the *t*-plot method, and V_{total} = total pore volume at $P/P_0 = 0.90$.

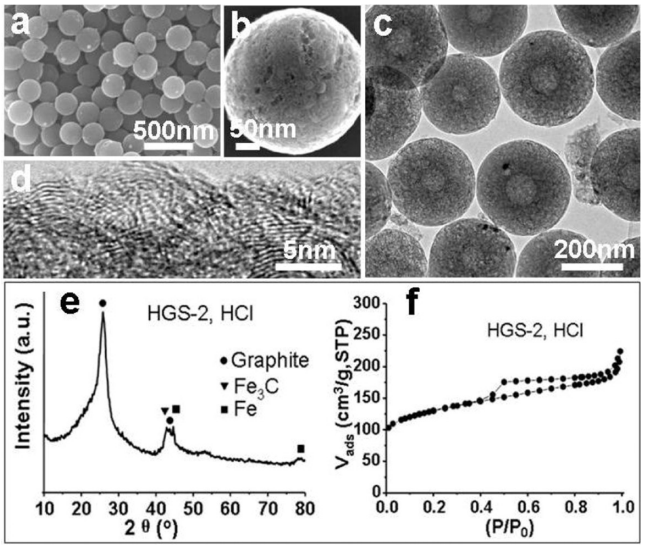

Figure 5. SEM (a, b) and TEM (c, d) images, XRD pattern (e), and N_2 sorption isotherm (f) of HGS-2 after HCl (37%) leaching.

shell thickness of HGSs are about 280 and 100 nm, respectively, both of which are greater than those of HPS-2 and HCS-2. This may be caused by the formation of mesopores in the shell. Moreover, the growth of graphitic carbons appeared strictly confined within the shell. This same phenomenon has previously been observed by us.[49] The graphitized nature of this sample was also confirmed by XRD analysis. Figure 5e shows its XRD pattern displaying typical reflections of well-developed graphitic carbon and weak reflections of Fe and Fe_3C. The particle sizes of the Fe particles were estimated to be ~20 nm by the Scherrer equation. The content of Fe_2O_3 determined by TG in air is about 2.73 wt % (Figure S6e, Supporting Information). That corresponds to 1.91 wt % Fe.

The N_2 sorption isotherm of the sample in Figure 5f is of type IV, indicating the mesoporous feature of the spheres. The pore size distribution of this sample is shown in Figure S6c (Supporting Information). This is in good agreement with the TEM and SEM images. Its specific surface area and total pore volume are 450 $m^2\ g^{-1}$ and 0.27 $cm^3\ g^{-1}$, respectively. This sample shows advantageous properties such as a hollow structure in the nanometer range, graphitic nature, and a high surface area for potential use as an electrode material.

3.3. Highly Active Hollow Colloidal Catalyst (HCS-Ag) for the Reduction of 4-Nitrophenol. In principle, various metal

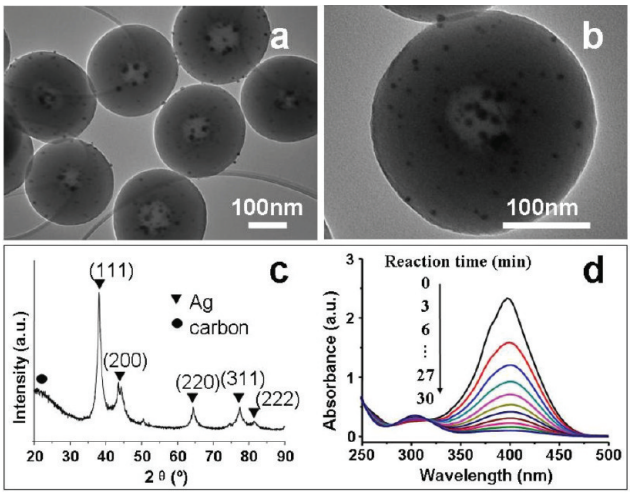

Figure 6. TEM images (a, b) and XRD pattern (c) of HCS-Ag. (d) UV−vis absorption spectra of the reduction of 4-nitrophenol by $NaBH_4$ in the presence of HCS-Ag.

cations can be introduced into the HPSs, which can then be engineered to fabricate colloidal catalysts with a high dispersion of nanoparticles as active species. Herein, as an example, Ag^+ was introduced into HPSs through an ion-exchange process. Followed by a pyrolysis step, catalyst HCS-Ag was obtained. Parts a and b of Figure 6 show the TEM images of this product. Interestingly, a large number of Ag particles are dispersed throughout the entire HCS-Ag sample. From the TEM image, by measuring a minimum of 200 Ag particles, about 80% of Ag particles fall in the size range of 5−8 nm. Figure 6c shows the XRD pattern of HCS-Ag. The main diffraction peaks at 38.1°, 44.3°, 64.4°, 77.3°, and 81.7° are indexed as (111), (200), (220), (311), and (222) reflections, which confirm the presence of silver (JCPDS file 04-0783) in the HCSs. The particle sizes of the Ag particles were estimated to be ~6.7 nm by the Scherrer equation. This is consistent with the TEM observation. The weight content of Ag determined by TG in air is about 8.5 wt % (Figure S6e, Supporting Information).

To test the catalytic activity of the product, the reduction of 4-nitrophenol (4-NP) by sodium borohydride was chosen as a model reaction. The yellow aqueous 4-NP mixed with $NaBH_4$ shows absorption at 400 nm due to the formation of 4-nitrophenolate.[52] After addition of a small amount (about 0.06 mg) of the HCS-Ag catalyst, the absorption peak at 400 nm significantly decreases as the reaction proceeds; meanwhile, a new peak appears at 295 nm and gradually increases, revealing the reduction of 4-NP to form 4-aminophenol (4-AP) (Figure 6d).[52,53] After 30 min, the absorption peak at 400 nm disappeared completely, indicating a total conversion of 4-NP. As a control experiment, HCS-2 without Ag nanoparticles was used as the catalyst. It turned out that no change in the absorption was determined even after standing for 2 h, indicating that the reduction does not proceed without Ag nanoparticles. This in turn confirmed that the colloidal HCS-Ag is an active catalyst for 4-nitrophenol reduction.

4. CONCLUSIONS

We have developed a novel and generalizable synthesis for diverse, functionalizable, and structurally stable hollow polymer

dx.doi.org/10.1021/cm2018168 |*Chem. Mater.* 2011, 23, 4537–4542

and carbon nanospheres, by utilization of the weak acid−base interaction (between carboxylate anion and ammonium ion) induced self-assembly under hydrothermal conditions. The diameter of hollow polymer nanospheres and the core sizes can be adjusted by changing the reaction conditions. Consequently, the sizes of the hollow carbon and graphitized nanospheres are also variable. The surface areas of the hollow carbon spheres can be enlarged by CO_2 activation while still retaining a spherical and hollow shape. More importantly, the highly functionalized HPSs can be further engineered to fabricate active colloidal catalyst, as demonstrated by the Ag nanoparticle (6.7 nm) doped carbonaceous hollow nanospheres. We believe that this work provides a simple and effective recipe for the designed synthesis of a wide range of novel hollow nanospheres containing specific noble metal (e.g., Pt, Pd, Au, etc.) nanoparticles for various targeted application fields, such as catalysis, drug delivery, lithium batteries, fuel cell electrodes, and hydrogen storage.

■ ASSOCIATED CONTENT

Supporting Information. Figures showing the dynamic light scattering results, TEM images, photographs, TG curves, FT-IR spectrum, pore size distributions, and N_2 sorption isotherm of the resultant samples (PDF). This material is available free of charge via the Internet at http://pubs.acs.org.

■ AUTHOR INFORMATION

Corresponding Author
*E-mail: anhuilu@dlut.edu.cn. Phone/fax: +86-411-84986112.

■ ACKNOWLEDGMENT

This project was supported by the National Natural Science Foundation of China (Grants 20873014 and 21073026) and the Program for New Century Excellent Talents in University of China (Grant NCET-08-0075).

■ REFERENCES

(1) Wang, Y.; Bansal, V.; Zelikin, A. N.; Caruso, F. *Nano Lett.* **2008**, *8*, 1741.
(2) Guo, L.; Zhang, L.; Zhang, J.; Zhou, J.; He, Q.; Zeng, S.; Cui, X.; Shi, J. *Chem. Commun.* **2009**, 6071.
(3) Kim, J. Y.; Yoon, S. B.; Yu, J.-S. *Chem. Commun.* **2003**, 790.
(4) Ikeda, S.; Ishino, S.; Harada, T.; Okamoto, N.; Sakata, T.; Mori, H.; Kuwabata, S.; Torimoto, T.; Matsumura, M. *Angew. Chem., Int. Ed.* **2006**, *45*, 7063.
(5) Valdes-Solis, T.; Valle-Vigon, P.; Sevilla, M.; Fuertes, A. B. *J. Catal.* **2007**, *251*, 239.
(6) Fuertes, A. B.; Sevilla, M.; Valdes-Solis, T.; Tartaj, P. *Chem. Mater.* **2007**, *19*, 5418.
(7) Fang, B.; Kim, M.; Kim, J. H.; Yu, J.-S. *Langmuir* **2008**, *24*, 12068.
(8) Fuertes, A. B.; Valdes-Solis, T.; Sevilla, M. *J. Phys. Chem. C* **2008**, *112*, 3648.
(9) Chai, G. S.; Yoon, S. B.; Kim, J. H.; Yu, J.-S. *Chem. Commun.* **2004**, 2766.
(10) Fang, B.; Kim, M.; Yu, J.-S. *Appl. Catal., B* **2008**, *84*, 100.
(11) Yang, M.; Ma, J.; Zhang, C.; Yang, Z.; Lu, Y. *Angew. Chem., Int. Ed.* **2005**, *44*, 6727.
(12) Yang, M.; Ma, J.; Ding, S.; Meng, Z.; Liu, J.; Zhao, T.; Mao, L.; Shi, Y.; Jin, X.; Lu, Y.; Yang, Z. *Macromol. Chem. Phys.* **2006**, *207*, 1633.
(13) White, R. J.; Tauer, K.; Antonietti, M.; Titirici, M.-M. *J. Am. Chem. Soc.* **2010**, *132*, 17360.
(14) Wu, J.; Hu, F.; Hu, X.; Wei, Z.; Shen, P. K. *Electrochim. Acta* **2008**, *53*, 8341.
(15) Jing, J.; Ding, S.; Zhang, C.; Chen, C.; Rao, X.; Dang, G.; Yang, Z.; Zhou, H. *Mater. Chem. Phys.* **2009**, *116*, 330.
(16) Li, Y.; Chen, J.; Xu, Q.; He, L.; Chen, Z. *J. Phys. Chem. C* **2009**, *113*, 10085.
(17) Li, L.; Song, H.; Chen, X. *Carbon* **2006**, *44*, 587.
(18) Lv, H.; Lin, Q.; Zhang, K.; Yu, K.; Yao, T.; Zhang, X.; Zhang, J.; Yang, B. *Langmuir* **2008**, *24*, 13736.
(19) Jang, J.; Ha, H. *Langmuir* **2002**, *18*, 5613.
(20) Yoon, S. B.; Sohn, k.; Kim, J. Y.; Shin, C. H.; Yu, J. S.; Hyeon, T. *Adv. Mater.* **2002**, *14*, 19.
(21) Kamata, K.; Lu, Y.; Xia, Y. N. *J. Am. Chem. Soc.* **2003**, *125*, 2384.
(22) Xia, Y.; Mokaya, R. *Adv. Mater.* **2004**, *16*, 886.
(23) Zheng, T.; Zhan, J.; Pang, J.; Tan, G. S.; He, J.; McPherson, G. L.; Lu, Y.; John, V. T. *Adv. Mater.* **2006**, *18*, 2735.
(24) Su, F.; Zhao, X. S.; Wang, Y.; Wang, L.; Lee, J. Y. *J. Mater. Chem.* **2006**, *16*, 4413.
(25) Ikeda, S.; Tachi, K.; Ng, Y. H.; Ikoma, Y.; Sakata, T.; Mori, H.; Harada, T.; Matsumura, M. *Chem. Mater.* **2007**, *19*, 4335.
(26) Joo, J. B.; Kim, P.; Kim, W.; Kim, J.; Kim, N. D.; Yi, J. *Curr. Appl. Phys.* **2008**, *8*, 814.
(27) Wang, Y.; Su, F.; Lee, J. Y.; Zhao, X. S. *Chem. Mater.* **2006**, *18*, 1347.
(28) Xia, Y.; Yang, Z.; Mokaya, R. *J. Phys. Chem. B* **2004**, *108*, 19293.
(29) Wang, Y.; Price, A. D.; Caruso, F. *J. Mater. Chem.* **2009**, *19*, 6451.
(30) Lou, X. W.; Deng, D.; Lee, J. Y.; Archer, L. A. *Chem. Mater.* **2008**, *20*, 6562.
(31) Cheng, D.; Xia, H.; Chan, H. S. O. *Nanotechnology* **2006**, *17*, 1661.
(32) Schneider, G.; Decher, G. *Nano Lett.* **2004**, *4*, 1833.
(33) Antipov, A. A.; Shchukin, D.; Fedutik, Y.; Petrov, A. I.; Sukhorukov, G. B.; Mohwald, H. *Colloids Surf., A* **2003**, *224*, 175.
(34) Zhang, W.-M.; Hu, J.-S.; Guo, Y.-G.; Zheng, S.-F.; Zhong, L.-S.; Song, W.-G.; Wan, L.-J. *Adv. Mater.* **2008**, *20*, 1160.
(35) Sun, Z.; Bai, F.; Wu, H.; Schmitt, S. K.; Boye, D. M.; Fan, H. *J. Am. Chem. Soc.* **2009**, *131*, 13594.
(36) Chen, D.; Jiang, M. *Acc. Chem. Res.* **2005**, *38*, 494.
(37) Sun, X.; Li, Y. *J. Colloid Interface Sci.* **2005**, *291*, 7.
(38) Wen, Z.; Wang, Q.; Zhang, Q.; Li, J. *Electrochem. Commun.* **2007**, *9*, 1867.
(39) Yi, C.; Chien, C.; Hsu, C. H.; Lee, T. Y.; Liu, C. W.; Wu, S. H.; Lin, H. P.; Tang, C. Y.; Lin, C. Y. *Eur. J. Inorg. Chem.* **2007**, 3798.
(40) Zhou, C. Q.; Han, J.; Song, G.; Guo, R. *J. Polym. Sci., Part A: Polym. Chem.* **2008**, *46*, 3563.
(41) Huang, H.; Remsen, E. E.; Kowalewski, T.; Wooley, K. L. *J. Am. Chem. Soc.* **1999**, *121*, 3805.
(42) Han, J.; Song, G.; Guo, R. *Adv. Mater.* **2006**, *18*, 3140.
(43) Han, J.; Song, G.; Guo, R. *Chem. Mater.* **2007**, *19*, 973.
(44) McDonald, C. J.; Bouck, K. J.; Chaput, A. B.; Stevens, C. J. *Macromolecules* **2000**, *33*, 1593.
(45) Jinish Antony, M.; Jayakannan, M. *J. Phys. Chem. B* **2010**, *114*, 1314.
(46) Zhang, L.; Wan, M. *Adv. Funct. Mater.* **2003**, *13*, 815.
(47) Zoldesi, C. I.; Imhof, A. *Adv. Mater.* **2005**, *17*, 924.
(48) Cui, J.; Wang, Y.; Postma, A.; Hao, J.; Hosta-Rigau, L.; Caruso, F. *Adv. Funct. Mater.* **2010**, *20*, 1625.
(49) Lu, A.-H.; Li, W.-C.; Hao, G.-P.; Spliethoff, B.; Bongard, H.-J.; Schaack, B. B.; Schüth, F. *Angew. Chem., Int. Ed.* **2010**, *49*, 1615.
(50) Fiorilli, S.; Onida, B.; Bonelli, B.; Garrone, E. *J. Phys. Chem. B* **2005**, *109*, 16725.
(51) Lu, A.-H.; Li, W.-C.; Salabas, E. L.; Spliethoff, B.; Schüth, F. *Chem. Mater.* **2006**, *18*, 2086.
(52) Pradhan, N.; Pal, A.; Pal, T. *Langmuir* **2001**, *17*, 1800.
(53) Tang, S.; Vongehr, S.; Meng, X. *J. Phys. Chem. C* **2010**, *114*, 977.